

DYNAMICS OF THE GLOBULAR CLUSTER SYSTEM ASSOCIATED WITH M87 (NGC 4486). I.
NEW CFHT MOS SPECTROSCOPY AND THE COMPOSITE DATABASE

DAVID A. HANES^{1,2,3,4}, PATRICK CÔTÉ^{1,5,6,7}, TERRY J. BRIDGES^{1,3,8,9}, DEAN E.
MCLAUGHLIN^{1,10,11}, DOUG GEISLER^{12,13,14}, GRETCHEN L.H. HARRIS¹⁵, JAMES E. HESSER⁴,
MYUNG GYOON LEE¹⁶

Accepted for Publication in the Astrophysical Journal

ABSTRACT

We present a comprehensive database of kinematic, photometric and positional information for 352 objects in the field of M87 (NGC 4486), the central giant elliptical galaxy in the Virgo cluster; the majority of the tracers are globular clusters associated with that galaxy. New kinematic information comes from multi-slit observations with the Multi-Object Spectrograph (MOS) of the Canada-France-Hawaii Telescope (CFHT), an investigation which has added 96 new velocities to and confirmed many of the earlier values in a pre-existing dataset of 256 velocities published elsewhere. The photometry, consisting of magnitudes and colors in the Washington (T_1 , C- T_1) system, is based on CCD observations made at the Cerro Tololo Inter-American Observatory (CTIO) and the Kitt Peak National Observatory (KPNO). The composite database represents the largest compilation of pure Population II dynamical tracers yet identified in any external galaxy; moreover, it extends to larger spatial scales than have earlier investigations. The inclusion of photometric information allows independent study of the distinct red and blue sub-populations of the bimodal GCS of M87. In a companion paper (Côté et al. 2001), we use this powerful dataset to analyse the present dynamical state of the M87 globular cluster system, and consider the question of its interaction and formation history.

Subject headings: clusters: globular, galaxy formation

1. INTRODUCTION

The use of globular clusters as dynamical tracers of galaxy halos, both within and outside the Milky Way, has a long and important history. Their importance transcends that of mere descriptors of the present mass distribution and dynamical state of the parent galaxy: their extreme ages and ranges of chemical composition, and the evident correlations between these attributes and cluster position and kinematics, make them powerful fossil tracers of the formation and interaction history of galaxies. The concept of a monolithic galaxy formation process (Eggen, Lynden-Bell & Sandage 1962), with attendant dissipation and chemical enrichment, has been supplanted in recent years through the recognition of evidently more complex histories. The discovery of bimodal color distributions in the globular cluster systems (GCSs) of many elliptical galaxies, for instance, has invigorated theoretical investigations into the importance of (inter alia) merger events (Ashman & Zepf 1992), multi-modal star formation histories (Harris, Harris & McLaughlin 1998) and hierarchical growth (Côté, Marzke & West 1998) in the galaxy formation process. These issues are explored in more depth in our companion paper (Côté et al. 2001).

The promise of spectroscopic studies of GCSs is nowhere more evident than in external galaxies, within which globular clusters may serve as luminous dynamical test particles at galactocentric radii where the halo surface brightness is impractically faint. Moreover, they are sufficiently numerous that reasonably robust statistical analyses can be carried out,

¹Visiting Astronomer, Canada-France-Hawaii Telescope, operated by the National Research Council of Canada, the Centre National de la Recherche Scientifique of France, and the University of Hawaii

²Department of Physics, Queen's University, Kingston ON Canada K7L 3N6

³Anglo-Australian Observatory, P.O. Box 296, Epping NSW 1710, Australia

⁴Dominion Astrophysical Observatory, Herzberg Institute of Astrophysics, National Research Council, 5071 West Saanich Road, Victoria BC V9E 2E7, Canada

⁵Department of Physics and Astronomy, Rutgers University, New Brunswick, NJ 08854, USA

⁶California Institute of Technology, Mail Stop 105-24, Pasadena CA 91125 USA

⁷Sherman M. Fairchild Fellow

⁸Royal Greenwich Observatory, Madingley Road, Cambridge, CB3 0EZ, UK

⁹Institute of Astronomy, Madingley Road, Cambridge, CB3 0HA, UK

¹⁰Department of Astronomy, University of California, 601 Campbell Hall, Berkeley CA 94720-3411 USA

¹¹Hubble Fellow

¹²Grupo de Astronomía, Dpto. de Física, Universidad de Concepción, Casilla 160-C, Concepción, Chile

¹³Visiting Astronomer, Cerro Tololo Inter-American Observatory, which is operated by AURA, Inc., under cooperative agreement with the National Science Foundation

¹⁴Visiting Astronomer, Kitt Peak National Observatory, which is operated by AURA, Inc., under cooperative agreement with the National Science Foundation

¹⁵Department of Physics, University of Waterloo, Waterloo ON Canada N2L 3G1

¹⁶Astronomy Program, SEES, Seoul National University, Seoul 151-742, Korea

at least in principle. Until recently, however, heroic efforts were required to establish even limited datasets: the elliptical galaxies known to possess large GCSs (Hanes 1977) typically lie at Virgo-like distances, and spectroscopic investigations of their faint ($V \geq 19$ mag) globular clusters were at the limits of the available instrumentation; see for instance Mould et al. (1990).

The development of multi-spectroscopic instruments, such as the MOS at the Canada-France-Hawaii Telescope, has made feasible studies once beyond the grasp of 4-metre class telescopes: these instruments provide not just a considerable multiplex advantage, but also the benefits of highly efficient optical throughputs at superb observing sites. Such considerations motivated the extensive studies reported in Cohen and Ryzhov (1997) and Cohen (2000), who investigated the M87 GCS using the LRIS multi-slit spectroscopic instrument at the Keck Telescope. The data provided therein have been variously interpreted (Cohen and Ryzhov 1997; Kissler-Patig and Gebhardt 1998; Cohen, Ryzhov and Blakeslee 1998), but suffer both from the somewhat limited spatial coverage and a lack of color information which would allow independent analyses of the GCS sub-populations. In the present paper, we report the results of observations carried out at the CFHT, one in which we have been able to extend the spatial coverage, amplify the dataset by some 40% in total size, and provide the photometric information which will permit the comprehensive analysis reported in Côté et al. (2001).

2. TARGET IDENTIFICATION AND PHOTOMETRY

The globular cluster system associated with M87 has been the subject of a number of photometric investigations. In several of these (Hanes 1977; Strom et al. 1981; Harris 1986; McLaughlin, Harris and Hanes 1994; Geisler, Lee and Kim 2001) the emphasis has been upon the determination and analysis of the global photometric properties, cluster luminosity function, or spatial distribution of the system. Recent HST studies (e.g., Whitmore et al. 1995; Elson and Santiago 1996; Kundu et al. 1999) have mainly focussed on the *central* properties of the M87 globular cluster system (GCS). For instance, from the V-I colors of roughly one thousand globular clusters in the center of M87, Whitmore et al. (1995) and Elson and Santiago (1996) were the first to present unambiguous evidence for a bimodal color distribution – a ubiquitous feature among giant elliptical galaxies, and one which has important implications for galaxy formation models.

Indeed, the principal aim of the present study is to create a database which permits a subsequent dynamical analysis of the system and its sub-components, whether selected by color or position, in analyses intended to address the question of M87's formation history (Côté et al. 2001). Clearly, unambiguous target positions and precise multi-color photometry are necessary if this goal is to be realized. In this section, we describe the foundation on which we have built our final optimal dataset.

2.1. *Strom et al (1981)*

Strom et al. (1981), hereinafter S81, analysed microdensitometer scans of a set of deep KPNO 4-metre prime focus plates in three colors (UBR); they identified 1728 candidate globular clusters associated with M87. In subsequent spectroscopic studies (Mould, Oke and Nemeč 1987; Huchra and Brodie 1987; Mould et al. 1990; Cohen and Ryzhov 1997; Cohen, Blakeslee and Ryzhov 1998; Cohen 2000), the practice has been to identify targets by their S81 numbers, a convention which we will continue where possible (but see Section 2.3).

The S81 tabulations, although extensive, are inconvenient in one respect. Their X and Y positional entries (which we will hereafter denote with the symbols SX and SY) are in units of arcseconds relative to a reference point near the SE plate corner; as a consequence, they lack an absolute astrometric calibration. To remedy this, we have carried out an astrometric calibration of the S81 tabulations: to an rms precision of about one arcsecond in each coordinate, the SX and SY coordinates tabulated by S81 are related to right ascension and declination according to:

$$R.A.(2000) = 12^h + 30^m + ((1187.7 - 0.0244SX - 1.0242SY)/15)^s, \quad (1)$$

$$\delta(2000) = 12^\circ + (994.8 + 1.0007SX - 0.0249SY)'' . \quad (2)$$

The M87 galaxy center itself, which is located at $RA = 12^h 30^m 49^s.4$, $\delta = +12^\circ 23' 28''$ (2000), lies at $(SX, SY) = (424, 426)$ in the S81 system. The SY term in Equation 1 can be recognized as $1.000/\cos(\delta)$, with $\delta \sim 12^\circ 23'$; along with the SX term in Equation 2, this confirms the precise correctness of the plate scale adopted by S81. The small cross terms indicate that the S81 coordinates were slightly rotated (by $\sim 1^\circ.4$) relative to the cardinal directions on the sky.

In Table 1, we present a summary tabulation of the positional data for all the targets in the M87 field for which spectroscopically derived velocities are now known, whatever the source. (We postpone a discussion of the photometric and kinematic data in the table until Section 2.4 and Section 4.) In Table 1, the first column represents the S81 running number, amended when necessary (or newly defined) for the reasons described in Section 2.3. Subsequent columns present the (SX, SY) coordinates (columns 2,3); the astrometrically-determined target right ascension and declination (columns 4-5); and the offsets with respect to the M87 nucleus, measured in seconds of arc positively to the East (column 6) and the North (column 7).

2.2. *Geisler, Lee and Kim 2001*

In Côté et al. (2001), we analyse the dynamical behaviour of the red and blue sub-populations of the M87 globular cluster system. Such an analysis requires not just photometry of the several hundred dynamical tracers for which we now have velocities, but also a broader understanding of the separate *surface density profiles* of the two sub-populations.

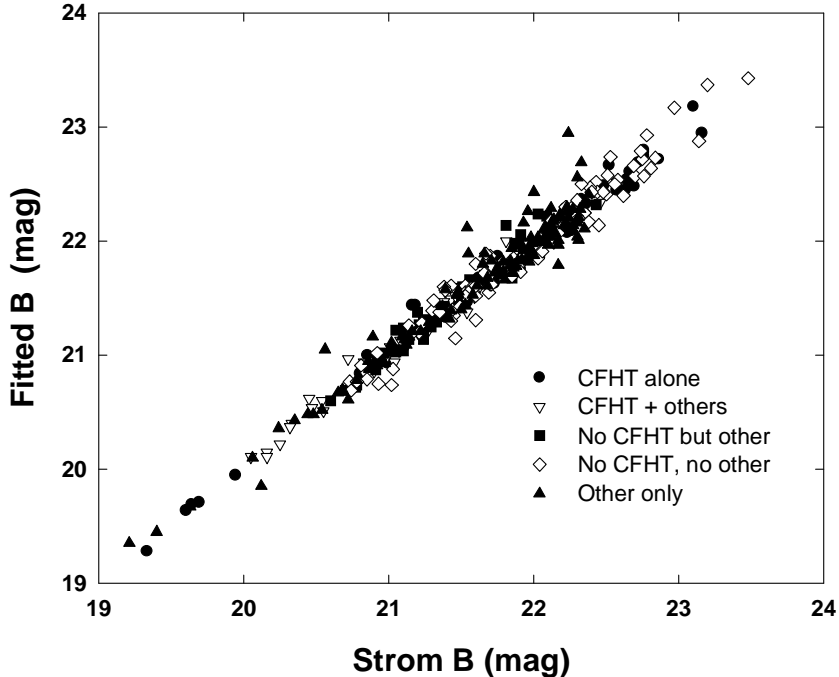


FIG. 1.— A comparison of the (C,C-T₁) CCD photometry with the S81 photographic B photometry, using the transformation given in the text, equation (3). The symbols represent: objects with CFHT velocities but no others reported (filled circles); objects with velocities from CFHT and elsewhere (open triangles); objects unsuccessfully targeted at CFHT but with velocities from elsewhere (filled squares); objects unsuccessfully targeted at CFHT and with no published velocity (open diamonds); and objects not studied at CFHT but with published velocities from other studies (filled triangles).

Unfortunately, the S81 photographic dataset is neither precise enough in its photographically-determined colors nor deep enough to define sufficiently large samples for this purpose. Indeed, many of the relatively bright spectroscopic targets themselves lack the precise colors necessary for their confident classification into the ‘red’ and ‘blue’ sub-populations. Moreover, there are occasional ambiguities in the target list; see Section 2.3.

The necessary information comes, however, from Geisler, Lee and Kim (2001), who have carried out deep photometry in the Washington photometric system in the field of M87. Their dataset was produced from direct CCD images taken at the prime focus of the KPNO 4-metre telescope. Using this extensive tabulation, we have cross-identified as many as possible of our spectroscopic targets and those previously studied by Cohen and Ryzhov (1997), Cohen (2000), and Mould et al. (1990), extracting the T₁ magnitudes and C-T₁ colors which are shown in our final composite tabulation (see Section 2.4). (It is important to note that the photometric data in the pre-publication tabulations provided by Geisler, Lee and Kim (2001) may yet be subject to minor revisions of individual data points. We do not expect such revisions to materially affect any of the analysis described in Côté et al. (2001).)

Even with the inclusion of the Geisler, Lee and Kim (2001) data, however, a number of our spectroscopic targets lacked essential color information, primarily because the direct images of Geisler, Lee and Kim (2001) were slightly offset from the center of M87. As a consequence, a few dozen objects for which we obtained good spectra lay beyond the bounds of the photometric dataset. To make up for this deficiency, we acquired additional direct frames of the field at the prime focus of the CTIO 4-metre telescope in March 2000, using C and R filters in front of the CCD mosaic camera. Photometric calibration was accomplished through the study of objects common to both studies; in this way, the (R, C-R) magnitudes and colors were reliably reduced to the Washington (T₁, C-T₁) system. In the end, we were able to determine the necessary colors and magnitudes for essentially all of the objects studied spectroscopically, with a few exceptions to be discussed later. At the relatively bright magnitude levels for objects for which we have reliable velocities, the photometric precision is typically $\pm 0^m.02$ or better in both T₁ and (C-T₁).

As Geisler (1996) demonstrated, reliable transformations can be established from the Washington (T₁, C-T₁) system to UBVRI with an rms scatter of about 0.05 mag in photoelectric determinations. In Figure 1, we compare the B photographic photometry tabulated by S81 to that derived from the CCD (T₁, C-T₁) study, with the datapoints restricted to those for which there is absolutely no ambiguity about target identification (see Section 2.3). A straightforward least-squares analysis yields a best-fit given by:

$$B_{fitted} = 1.069(C) - 0.419(C - T_1) - 1.038. \quad (3)$$

Although the leading coefficient reveals that there is a small scale error in the photographic photometry, the tightness of the relationship (about which there is an rms scatter of ~ 0.1 mag) is a testament to the quality of the photographic photometry presented by S81. (The various symbols are explained in the figure caption.) Almost without exception, the filled triangles which lie above the mean relationship represent targets which are projected against the central parts of

M87, where the background is both bright and rapidly spatially variable.

2.3. A Revised Numbering Scheme

Extensions to the S81 numbering scheme were introduced by Cohen and Ryzhov (1997) and Cohen (2000) to permit the inclusion of targets not appearing in the original photographic study. We need now to further extend the S81 numbering scheme, for two reasons. The first is that the study reported here extends to spatial scales beyond those of S81. But we have also discovered, through close inspection of our direct frames, that some of the S81 identifications do not correspond to unique targets. The tabulated coordinates for Strom 978, for instance, point to a location in the middle of a very close triplet of objects, apparently merged in the S81 photographic analysis.

Our objective is to provide a definitive database for subsequent analysis. For absolute clarity, therefore, we have amended the numbering scheme in ways which accommodate new objects, reflect the status of ambiguous targets, and indicate the availability and reliability of the necessary photometry. In Table 2, we present a succinct target-by-target summary of the considerations which motivate the amendments.

For all objects with published velocities, we now adopt a set of identification numbers which adhere to the following conventions:

Targets numbered below 2000 (289 of them): are those which retain their original S81 numbers to indicate that they are unambiguously identified and that we have good photometry in the ($T_1, C-T_1$) system.

Targets numbered in the low 5000s (7 of them): were introduced by Cohen and Ryzhov (1997) to represent objects not found in S81 (typically because they were rather close to the galaxy center and thus projected onto a bright background). Velocities were reported for seventeen such objects, although the target numbers ranged from 5001 to 5028; presumably the missing ones refer to slitlet positions which yielded no useful spectra. In Cohen and Ryzhov (1997), the positions of these objects were given in terms of EW and NS offsets relative to Strom 928.

We have found an unambiguous and precise ($\leq 0''.3$) coordinate transformation which maps nine of these objects, along with Strom 928 itself, into bright targets in the Geisler, Lee and Kim (2001) photometric database, and are completely confident of their identifications. Of these nine objects, seven retain the identification numbers introduced by Cohen and Ryzhov (1997) to reflect this complete knowledge.

Two of the identification numbers, 5024 and 5026, are redundant. It appears that the duplication of a couple of slit positions passed unnoticed in the analysis of the masks used at the telescope by Cohen and Ryzhov (1997). Our astrometric analysis reveals that object 5026 corresponds to Strom 978 in Table 3 of Cohen and Ryzhov (1997), while object 5024 corresponds to the entry immediately following Strom 978, an unnumbered object described in a footnote as lying $6''.6$ to the East. This interpretation is confirmed by the good agreement in the velocities: Cohen and Ryzhov (1997) report $v = 1076$ and 1141 km/sec for objects 5024 and the unnamed target; meanwhile, they find $v = 1990$ and 1878 km/sec for objects 5026 and 978. For each pair, the measurements agree to well within the combined measurement errors estimated by Cohen and Ryzhov (1997), and we adopt unweighted average values in our final tabulation. The redundancy is complicated by the fact that the targets lie at the notional position of object 978, which is itself a close triplet of unresolved objects. (Indeed, Cohen and Ryzhov (1997) discovered the extra spectrum of their unnamed object serendipitously on the slit positioned on the other target.) We resolve the redundancy and reflect the ambiguity by renaming these objects as numbers 8005 (=5026/978) and 8006 (=5024/unnamed), a choice explained below.

Targets numbered in the upper 5000s (8 of them): represent the remaining “5000-series” targets introduced by Cohen and Ryzhov (1997), those for which we could find no counterpart in the Geisler, Lee and Kim (2001) data (although they appear on our direct images). All but one of these lie considerably closer to the galaxy center, and thus on much brighter backgrounds, than do those for which we have made secure identifications. To reflect the lack of photometric information, we renumber them in the upper 5000s through the simple expedient of adding 50 to the numbers used by Cohen and Ryzhov (1997). Although such targets can be used in undifferentiated analyses of the global dynamical state of the cluster system, they can of course not be assigned to one of the cluster sub-populations until new photometry is secured.

Targets numbered in the 6000s (2 of them): represent two new objects presented by Cohen (2000), with positions expressed in terms of offsets relative to Strom 176. Again we find secure identifications in the Geisler, Lee and Kim (2001) photometric dataset, and simply retain the numbers introduced by Cohen (2000).

Targets numbered in the 7000s (28 of them): represent, in a logical extension of the numbering scheme introduced by Cohen and Ryzhov (1997) and Cohen (2000), objects not appearing in the S81 tabulation but for which we have good photometry and reliable CFHT MOS velocities and positions. The inclusion of such objects stems from the fact that our mosaic of spectroscopic target fields extended beyond the boundaries of the S81 study.

Targets numbered from 8001 to 8008 (8 of them): represent objects which are found in the S81 dataset, but close inspection of which reveals that there are potential ambiguities in identification. Typically, such objects consist of small clumps of several unresolved sources which the S81 tabulations do not distinguish. Inspection of the MOS mask reveals which component was the precise spectroscopic target, and they are likewise cleanly resolved in the Geisler, Lee and Kim (2001) photometry. Such targets, therefore, can be used without qualm in the ensemble dataset.

Targets numbered from 8051 to 8056 (6 of them): represent objects which are also ambiguous in the S81 dataset but for which we can still confidently assign a photometric classification into the ‘blue’ or ‘red’ sub-population. For instance, Cohen and Ryzhov (1997) report a velocity for Strom 827 but did not record that the (SX,SY) coordinates in fact point to a close *pair* of unresolved objects. Without reference to the LRIS masks, we cannot know which of them was the spectroscopic target, but the Geisler, Lee and Kim (2001) photometry yields the information that both components

are clearly red (according to the criterion adopted in Côté et al. (2001)). Except for a very small uncertainty in the precise position, therefore, such targets can be used with confidence in the multi-color dynamical analysis described in the companion paper Côté et al. (2001).

Targets numbered in the low 9000s (2 of them): represent objects which are ambiguous in the S81 data set and for which we are unable to carry out a photometric classification. By contrast to the objects in the ‘high-8000’ series, these are typically double targets unresolved by S81 for which Keck velocities are reported by Cohen and Ryzhov (1997) or Cohen (2000) but for which there is a red and a blue component. Again, lacking access to the LRIS masks we are unable to determine which component provided the spectrum. Such tracers can be used in a global dynamical analysis (modulo a very small positional ambiguity) but cannot be used in the treatments of sub-populations identified by color.

Targets numbered in the high 9000s (3 of them): have no reliable photometry. One of these, number 9052, formerly Strom 868, is lost in an apparent cosmic ray event in the Geisler, Lee and Kim (2001) database; another, number 9051, is easily seen in our CFHT direct frames but not found in the Geisler, Lee and Kim (2001) tabulations. The third object, number 9053 (formerly Strom 881), lay outside the Geisler, Lee and Kim (2001) study, but unfortunately fell too near the edge of the additional direct frames acquired at CTIO for reliable photometry. Again, the velocities make these targets useful for a global analysis but not in any treatment which entails a split into sub-populations defined by color.

2.4. The Final Dataset: Photometry and Kinematics

In Table 1, in addition to the astrometric data, we present the composite photometric and kinematic dataset for all objects for which velocities are now known (but defer a discussion of the velocity determinations until the next section). Successive columns provide the magnitudes and colors in the Washington T_1 , (C- T_1) system (columns 8,9); the new CFHT MOS-based velocities and their associated formal uncertainties (column 10); and previously published velocities from studies at the Keck telescope (K00 = Cohen (2000); K97 = Cohen and Ryzhov (1997)) and elsewhere (M90 = Mould et al. (1990)) (columns 11-13).

3. CFHT MOS SPECTROSCOPY

3.1. Instrumentation and Methodology

We used the MOS (Multi-Object Spectrograph) on five dark nights (May 17-22 1996) at the f/8 Cassegrain focus of the Canada-France-Hawaii Telescope (CFHT). (An earlier scheduled run, in March 1995, was lost completely to a combination of island-wide power outages and bad weather.) The MOS instrument has been well described elsewhere (Le Fevre et al. 1994); in direct imaging mode, it consists of an f/8-f/2.75 focal-reducer which is used to reimagine the Cassegrain field through transfer optics onto a 2048x2048 CCD.

The STIS2 CCD which is used with MOS has 21 micron square pixels, yielding an image scale of 0.44 arcsec per pixel and full-field coverage of 15 x 15 arcmin, although the MOS optics and mask holders introduce a vignetting which reduces this to an effective size of about 9.5 arcmin square in direct imaging mode. (See Table 3 for a brief summary of these and other important points.) Once acquired, the direct images are used in the design of masks containing slitlets overlying the desired spectroscopic targets. The entire process of designing, laser-cutting and inserting a mask into the four-position mask slide, and then aligning it to the target field, takes typically about an hour and a half.

Early on the first night of our run, we had difficulty in securing well-focussed images for mask design because of problems with the auto-focus software. Because of the less than optimal scheduling of the run (in late May), this meant that our principal field had set on Night 1 before we had designed, cut, and mounted the first masks. Thereafter, the operation ran smoothly, except that on Night 4 one of our masks was accidentally inserted into the holder slightly askew. The targets on only about half of the field lay on the slitlets, but still provided useful spectra; for the last night’s observations, we cut and mounted a new mask.

In designing the masks, we identified our targets first with reference to the V band data of McLaughlin, Harris and Hanes (1994); in more distant regions of the GCS, where no published CCD photometry exists, targets were selected solely on the basis of having a starlike appearance. Thanks to the unavailability of color information, our selection of targets necessarily included some which were unlikely to be globular clusters. (Indeed, the objects of extreme red color typically turn out to have M-dwarf spectra, as Cohen and Ryzhov (1997) also noted.) The value of having a pre-existing photometric dataset in multiplex investigations of this sort can scarcely be overstated. We will return to this point in our discussion of our attained efficiency.

For the dispersing element, we employed the B400 grism, which has a nominal dispersion of 3.6Å per 21-micron pixel and a zero-deviation wavelength of 5186Å, but inserted a pre-filter with a throughput from 4400Å to 5700Å. This strategy allowed us to include extra targets in the CCD field without overlapping any spectra. (Our most crowded field, for instance, had 104 slitlets.) In general, slitlets were designed to a length of eight to ten arcsec and were centrally placed on the targets; the local sky was thus well sampled on $\sim 5 - 6$ arcsec scales spanning most of the objects. Here and there, a number of somewhat shorter slitlets were used to allow the inclusion of additional targets.

In Figure 2, we present a montage of spectra for several objects: (a) the metal-poor Galactic globular cluster NGC 6205 (M13), for which $[\text{Fe}/\text{H}] = -1.54$; (b) the metal-rich Galactic globular cluster NGC 6356, with $[\text{Fe}/\text{H}] = -0.50$; (c) the M87 globular cluster Strom 8007, with $(T_1, \text{C}-T_1) = (19.46, 1.58)$; and (d) the M87 globular cluster Strom 859, with $(T_1, \text{C}-T_1) = (20.98, 1.30)$. The most prominent spectroscopic features are the Mgb triplet at $\sim 5170\text{Å}$ and $H\beta$ at 4861Å, although the cross-correlation techniques employed in the determination of velocities are of course sensitive to all features in the wavelength range.

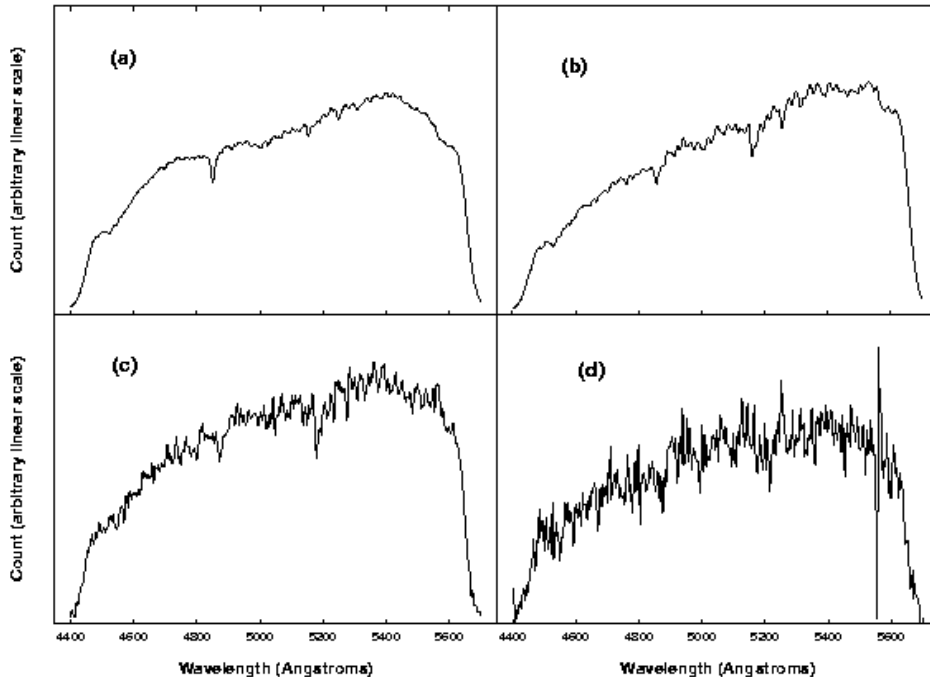


FIG. 2.— Reduced spectra for (a) NGC 6205 (M13), a Galactic globular cluster; (b) NGC 6356, a Galactic globular cluster; (c) Object 8007 in the M87 field, a target with $(T_1, C-T_1) = (19.46, 1.58)$; and (d) Object 859 in the M87 field, a target with $(T_1, C-T_1) = (20.98, 1.30)$. The derived heliocentric velocities for objects 8007 and 859 are $1183 \pm 32 \text{ km sec}^{-1}$ and $1064 \pm 91 \text{ km sec}^{-1}$ respectively.

3.2. Instrument Characterization and Calibration

The observing procedures were standard. In brief:

Approximately two dozen full bias frames were taken at various stages in the run. Halogen (continuum) lamps were used to illuminate the masks and were imaged both with and without the grism in place—the latter to provide an unambiguous identification between any slit and its intended target in the direct image of the galaxy field, and the former to allow the tracing of any geometric (principally pincushion) distortion in the MOS optics. These continuum lamp images also permit the determination of the uniformity of the slit width along its length (the slit function).

Helium and neon emission lamps were used to provide wavelength calibration for the spectra acquired. Wavelength-calibration frames were taken frequently, and always before any movement of the telescope to a new target or change in position of the MOS mask holder. During data reduction, the prominent night-sky line at $\sim 5577\text{\AA}$ was monitored as an external check on our wavelength calibration; its position was consistently as expected, typically to better than one-tenth of a pixel.

At opportune moments during the observing run, we acquired ten dark frames. These frames took on an unforeseen importance when we discovered that the MOS detector was registering a diffuse light leak from an unknown source within the instrument rack. Unfortunately, for the first three nights of the run this problem resisted a simple solution. Although the light leak displayed a degree of frame-to-frame variability, both in amplitude and in exact profile, subtracting an interactively scaled version of the average dark frame compensated fairly well for the contaminating light, leaving only small residual gradients. As will be shown, there are no indications of problems introduced as a result of this process: when we intercompare our velocities to those from independent studies, we find very good agreement. We are confident, therefore, that the our handling of the unwanted scattered light has introduced no significant systematic errors.

Inevitably, though, the subtraction of the unwanted light led to a degradation in the final spectroscopic signal-to-noise ratio in the affected fields. The effect of this is shown in Figure 3, in which we contrast the efficiencies of our velocity determinations in frames secured with (panel (a)) and without (panel (b)) the light leak. In the figure, filled symbols represent targets for which reliable velocities were determined; open symbols represent targets for which no good velocity could be derived. (The differently shaped symbols represent the different pointings of the telescope.) In dark conditions, the attained efficiency was almost exactly 50%; in the presence of the light leak, this was dramatically reduced (to about 30%), with an obvious loss of limiting magnitude. The figure also demonstrates that there are also some rather bright targets for which we failed to determine good velocities. In many cases, this is because of the very poor template mismatch between our calibrating spectrum (the globular cluster composite) and that of the target (often a recognizable M-star spectrum).

3.3. Velocity Templates

Spectra were acquired for radial velocity standard stars of appropriate spectral type (G8III, K2III) and for a number of Galactic globular clusters (NGCs 6171, 6205, 6356, 6402, 6528, 6624) spanning a range of metallicities. For the globulars, the telescope was made to nod slowly during the integration in order to sweep a single long slit across the face of the

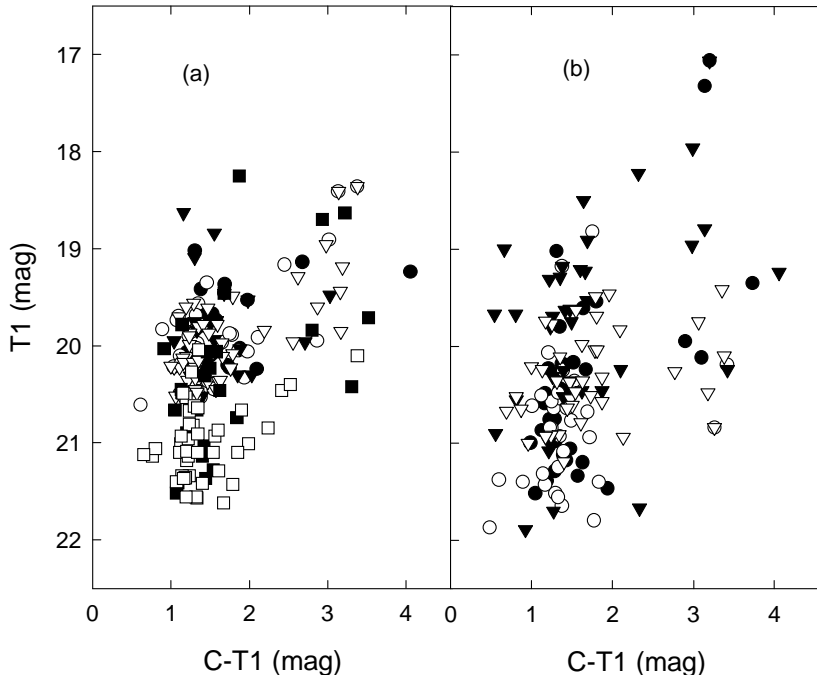


FIG. 3.— Color-magnitude diagrams in $(T_1, C-T_1)$ for targets in the M87 field for which good velocities were derived (filled symbols) or not (open symbols). Panel (a) corresponds to the three early pointings for which the observations were troubled by scattered light; panel (b) represents the two later pointings in which this was not a problem. The loss of efficiency and the attendant effect on our limiting magnitude are evident in panel (a).

target; after wavelength calibration and geometrical distortion corrections, the data were then further summed along the central parts of the slit to produce a final integrated spectrum. The extreme ends of the slit were used to determine the contribution attributable to sky light.

In Table 4, we summarize the important properties of the Galactic globular clusters observed as radial velocity templates. Experimentation revealed that considerably more reliable velocities resulted from their use (when cross-correlated one with another) than could be obtained when the bright standard stars were used as velocity standards. We attribute this to two factors: first, the Galactic globular clusters fill the slit uniformly, whereas the necessarily brief integrations on the very bright radial velocity stars may introduce systematic offsets if the stars lie slightly off the precise slit center. Secondly, the clusters have composite spectra, and are presumably better templates for one another – and, by extension, for the target clusters in M87 – than spectra of individual stars.

For these reasons, we elected to use only the Galactic globular clusters as velocity references. For each of them, an excellent high-signal-to-noise spectrum was reduced to the rest frame, and the spectra were then normalized and added to provide a standard spectrum with composite features spanning the range of likely globular cluster compositions. The cross-correlation analysis followed conventional practice; see Section 3.5.

3.4. The M87 Mosaic

With the objective of studying the M87 GCS to large galactocentric distances, we secured a mosaic of five direct images on the first night: one central pointing; and four more offset radially by about 5.4 arcmin in each of the NE, NW, SE, and SW directions (520 pixels, or 3.84 arcmin, along each of the cardinal directions). Given the field size of the MOS detector, this allowed overlap strips within which a number of targets were repeated; see Section 3.6. Moreover, the populous central field was visited twice, using two different masks but with several of the targets repeated. Unfortunately, time lost to bad weather and occasional technical problems prevented us carrying out any spectroscopic observations in the NE quadrant on any of the scheduled nights, but the other parts of the mosaic were well sampled. In Table 5, we present a summary description of the spectroscopic integrations carried out on the fields in our M87 mosaic.

3.5. Spectroscopic Data Reduction

The data reduction was carried out almost entirely within the well-known suite of IRAF¹⁷ common-user software. The process was straightforward but necessarily quite interactive, with the following principal stages:

Every frame was preprocessed in the usual way. The overclocked regions were evaluated and subtracted; the median bias was removed; and an appropriately scaled ‘dark’ frame was subtracted if necessary. Cosmic ray events were removed through a combination of the IRAF COSMICRAY task and special interactive software written expressly for the purpose.

Individual spectra were identified in the data frames with reference to the corresponding direct images of the target

¹⁷IRAF is distributed by the National Optical Astronomy Observatories, which are operated by the Association of Universities for Research in Astronomy, Inc., under contract to the National Science Foundation.

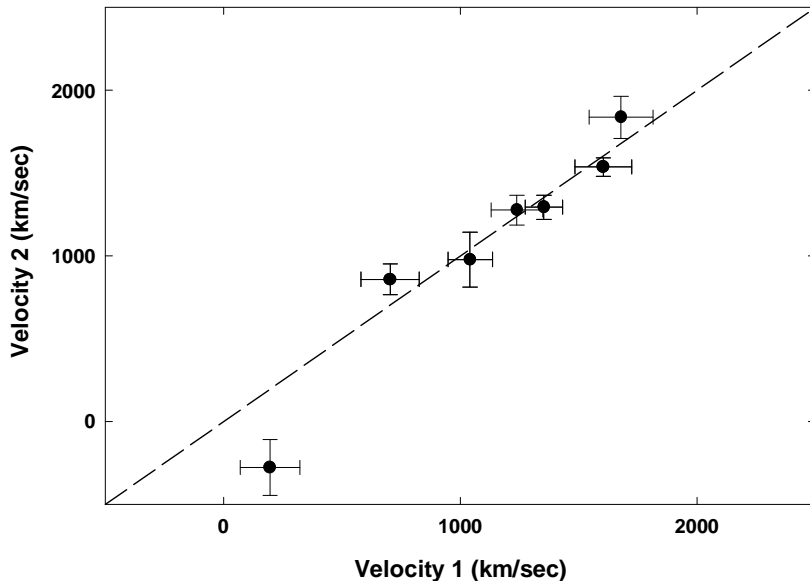


FIG. 4. — A comparison of velocities derived for targets studied on independent MOS masks; the error bars represent the formal uncertainties. In the various pairings, every one of the five masks employed is represented at least once. The broken line is the identity relationship.

fields and the illuminated masks. In the dispersed images, the typical slit length projected to less than 30 pixels ($13''$), with the spectra stretching about 300 pixels in the sense of the dispersion. Matched sub-frames of 40×320 pixels were removed from the spectroscopic frame, the emission lamp frame(s), and the dispersed halogen lamp (continuum) frame.

For each triad of such frames, the continuum spectrum was examined to see if any geometrical transformation was needed (typically a small rotation) to remove the effects of pincushion distortion. When necessary, this correction was applied to all three of the excised sub-frames to straighten the spectra.

The continuum spectrum was collapsed spectrally over the regions of highest signal to yield a high-precision estimate of the slit function. This was required for several of the spectra because of an occasional raggedness in the laser cutting of slitlets, a problem which has since been largely solved at the CFHT with the introduction of an auto-focus feature in the mask-cutting machinery. For the vast majority of the spectra, however, the data needed at most a modest correction for the slit function.

The remaining steps in the reduction were conventional: the definition of the location of the star along the slit; the determination of the level of and gradient in the sky (background) light; the wavelength calibration with reference to the corresponding arc frames; and so on. Optimal weighting was used in the sky subtraction, and the final sky-subtracted target spectra were put onto linear wavelength scales, preserving the original spectral resolution.

The final velocities and their respective uncertainties were determined by use of the IRAF FXCOR package, and were derived independently by two of us to allow separate assessments of the strength and significance of the derived cross-correlation peaks and the influence of residual cosmic ray traces and the like. Any objects which yielded significantly different velocities under these two treatments were given especially careful scrutiny; a few were rejected as untrustworthy. The median uncertainty of our CFHT/MOS velocities for the 109 confirmed globular clusters in our sample (see Paper II) is $103 \pm 20 \text{ km s}^{-1}$.

3.6. *The Velocity Precision Attained: Internal Comparisons*

Before comparing our derived velocities to those available from other studies, we carry out an intercomparison of those objects for which we derived reliable velocities from more than one mask. Unfortunately, there are not as many such targets as we had planned, thanks to the reduced success rates which we experienced on the masks afflicted by scattered light problems. Moreover, except for the repeated central pointings, the overlap regions were moderately close to the edges of the masks, in regions where slitlets were sometimes raggedly cut to such an extent that no useful spectrum could be derived even for a relatively bright object. In the last analysis, however, we have seven multiply-studied objects, with every mask represented at least once.

Figure 4 shows the quality of the systematic agreement. It can be seen that the velocities agree to within the formal uncertainties, except for a single low-velocity object for which the deviation from the identity line is still less than twice the combined errors. This intercomparison reassures us that there are no significant mask-to-mask zero-point or scale differences, and that our estimates of the formal uncertainties are realistic.

3.7. *The Velocity Precision Attained: External Comparisons*

Various studies (Huchra and Brodie 1987; Mould, Oke and Nemec 1987; Mould et al. 1990; Cohen and Ryzhov 1997; Cohen 2000) have reported velocities for the globular clusters associated with M87 (and inevitably for a number of the field stars and compact background galaxies in the field). The most comprehensive of these studies is that stemming from

the use of LRIS at the Keck Telescope, the first tabulations of which appeared in Cohen and Ryzhov (1997). These data were later augmented by the addition of five new datapoints (and two amendments) in Cohen, Blakeslee and Ryzhov (1998); another sixteen velocities (four of which repeat values from Cohen and Ryzhov (1997)) appeared in Cohen (2000). In total, these studies contribute 244 velocities for unresolved objects in the M87 field, so it is particularly important to test the systematic agreement of our own dataset with those measurements.

In Figure 5, therefore, we present a comparison of MOS-derived velocities, plotted with explicit error bars, with those tabulated in Cohen (2000) (upper panel; 8 objects) and Cohen and Ryzhov (1997) (lower panel; 48 objects). In each case, the broken line represents the identity relationship. The best-fit least-squares line, shown in solid, is not significantly different from the line of unit slope in either case. In the lower panel in particular, the formal linear regression is given by $v_{MOS} = 0.96 (v_{K97}) + 91 \text{ km sec}^{-1}$.

In the upper panel, there is a suggestion of a zero-point offset between the MOS velocities and those reported by Cohen (2000), in the sense that the MOS velocities are larger by $\sim 85 \text{ km sec}^{-1}$ on average; interestingly, for four repeated objects, the velocities reported by Cohen and Ryzhov (1997) are likewise numerically larger than those in Cohen (2000), by 62 km/sec in the mean, suggesting that the zero-point in the Cohen (2000) study may have an offset of about this magnitude relative to the Cohen and Ryzhov (1997) frame.

Although of much lower precision, the velocities tabulated by Mould et al. (1990) represent the heroic efforts of various researchers Huchra and Brodie 1987; Mould, Oke and Nemec 1987) whose observations predated the advent of multiplex devices such as MOS and LRIS. Perhaps surprisingly, not all of the rather bright targets which they studied have been repeated in subsequent programs, and these data points, suitably weighted to reflect their imprecision, may yet provide some leverage in dynamical analyses. As is shown in the separate panels of Figure 6, where the broken lines represent the identity relationship, there is moderately good systematic agreement between the velocities compiled in Mould et al. (1990) and those determined separately by Cohen and Ryzhov (1997) and in the present study. In the lower panel in particular, the formal regression solution is $v_{MOS} = 0.76 (v_{M90}) + 280 \text{ km sec}^{-1}$; it is shown as a solid line.

4. THE FINAL DATASET

In Figure 7, we plot the spatial distribution of *all objects for which velocities are now known in the M87 field*, clearly distinguished to represent the source of the information. (In Côté et al. (2001), we will of course restrict the dynamical analysis to just that [large] fraction of the sample which are *bona fide* globular clusters associated with M87.) As can be seen, the new MOS data are important not just insofar as they augment the database by some 40%, but also—and just as importantly—in that they extend the spatial coverage to larger galactocentric radii, a contribution which will be important in providing strong leverage in studies of the dynamical state of the globular cluster system of M87 (Côté et al. 2001). Unfortunately, as the figure makes clear, there is a paucity of datapoints in the Northeast quadrant. Nevertheless,

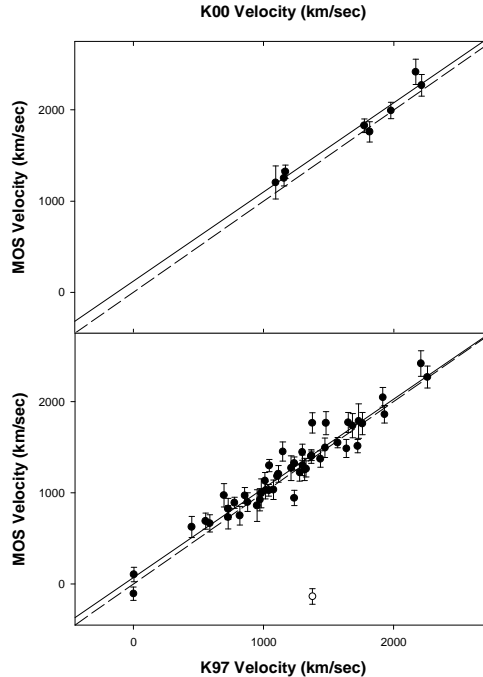


FIG. 5.— A comparison of the velocities determined with the CFHT MOS instrument and those from the studies of Cohen and Ryzhov (1997) (bottom panel; 48 objects in common) and Cohen (2000) (top panel; 8 objects in common). The formal CFHT error bars are shown. In each panel, the broken line represents the identity relationship, while the solid line is the formal least-squares fit to the data points. The open symbol in the bottom panel corresponds to Object 321, which may have been misidentified in Cohen and Ryzhov (1997); the point was not used in the regression analysis. [J.Cohen (2001, private communication) has now confirmed that the LRIS spectrum of Object 321 is that of an M star of low velocity, consistent with the MOS result.]

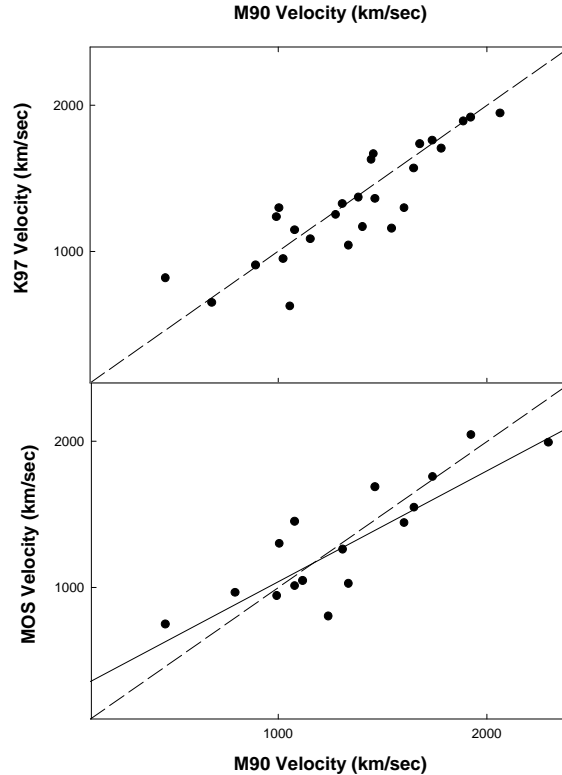


FIG. 6.— A comparison of the velocities tabulated by Mould et al. (1990) with those reported by Cohen and Ryzhov (1997) for objects in common. In each panel, the broken line is the identity relationship. In the lower panel, the solid line represents the formal best-fit linear regression.

the combination of photometric information, sufficiently precise velocities, and *sheer numbers* of dynamical tracers will allow an analytic treatment of unprecedented significance in this important subject area.

5. CONCLUSIONS

We have presented a comprehensive dataset which incorporates all known velocity tracers in the field of M87. The new observations described here have augmented the results of earlier studies by 40% in number (to a total of 352 objects) and have been shown to be in excellent systematic agreement with the earlier measurements. We have extended the spatial scale of the investigation to larger galactocentric radii than was formerly the case, and have also been able to provide precise CCD photometry in the Washington system for all but a few of the objects. Particular attention has been paid to the question of the unambiguous identification of all targets, the coordinates of which have moreover been put onto an absolute astrometric scale. In Côté et al. (2001), we present a dynamical study of the GCS of M87 and describe the implications and inferences in the context of galaxy formation and interaction history.

The research of DAH and GLHH is supported through grants from the Natural Sciences and Engineering Research Council of Canada. DAH is pleased to thank the Directors of the Dominion Astrophysical Observatory and the Anglo-Australian Observatory for their hospitality and support during a research sabbatical. PC gratefully acknowledges support provided by the Sherman M. Fairchild Foundation during the course of this work. DEM acknowledges support from NASA through grant number HF-1097.01-97A awarded by the Space Science Telescope Institute, which is operated by the Association of Universities for Research in Astronomy, Inc., for NASA under contract NAS5-26555. DG acknowledges financial support for this project received from CONICYT through Fundecyt grant 8000002, and from the Universidad de Concepción through research grant No. 99.011.025-1.0.

REFERENCES

- Ashman, K.M. and Zepf, S.E. 1992, *ApJ*, 384, 50
 Cohen, J.G. 2000, *AJ*, 119, 162
 Cohen, J.G., Blakeslee, J.P. and Ryzhov, A. 1998, *ApJ*, 496, 808
 Cohen, J.G. and Ryzhov, A. 1997, *ApJ*, 486, 230
 Côté, P., Marzke, R.O. and West, M.J. 1998, *ApJ*, 501, 554
 Côté, P., McLaughlin, D.E., Hanes, D.A., Bridges, T.J., Geisler, D., Merritt, D., Hesser, J.E., and Harris, G.L.H. 2001, *ApJ*, to be submitted.
 Eggen, O.J., Lynden-Bell, D. and Sandage, A.R. 1962, *ApJ*, 136, 748
 Elson, R.A.W. and Santiago, B.X. 1996, *MNRAS*, 278, 617
 Geisler, D. 1996, *AJ*, 111, 480.
 Geisler, D., Lee, M.G. and Kim, S.C. 2001, *in preparation*
 Hanes, D.A. 1977, *Mem.R.A.S.* 84, 45
 Harris, W.E. 1986, *AJ*, 91, 822
 Harris, W.E. 1996, *AJ*, 112, 1487
 Harris, W.E., Harris, G.L.H. and McLaughlin, D.E. 1998, *AJ*, 115, 1801
 Huchra, J.P. and Brodie, J.P. 1987, *AJ*, 93, 779
 Kissler-Patig, M. and Gebhardt, K. 1998, *AJ*, 116, 2237
 Kundu, A., Whitmore, B.C., Sparks, W.B., Macchetto, F.D., Zepf, S.E. and Ashman, K.M. 1999, *ApJ*, 513, 733
 Le Fevre, O., Crampton, D., Felenbok, P., and Monnet, G. 1994, *A&A*, 282, 325

McLaughlin, D.E., Harris, W.E. and Hanes, D.A. 1994, ApJ, 422, 486
Mould, J.R., Oke, J.B., and Nemec, J.M. 1987, AJ, 93, 53
Mould, J.R., Oke, J.B., de Zeeuw, P.T. and Nemec, J.M. 1990, AJ, 99, 1823

Strom, S.E., Forte, J.C., Harris, W.E., Strom, K.M., Wells, D.C. and Smith, M.G. 1981, ApJ, 245, 416
Whitmore, B.C., Sparks, W.B., Lucas, R.A., Macchetto, F.Duccio, and Biretta, J.A. 1995, ApJ, 454L, 73

FIG. 7.— The spatial distribution of objects of known velocity in the M87 field; North is up and East is to the left. The green filled circles represent new CFHT MOS measurements; the blue squares represent repeat measurements of previous determinations; and the red triangles represent all other published determinations.

TABLE 1
POSITIONS, PHOTOMETRY AND KINEMATICS.

ID	SX ^{''}	SY ^{''}	RA(2000)	Dec(2000)	$\Delta\alpha$ ^{''}	$\Delta\delta$ ^{''}	T ₁ (mag)	C-T ₁ (mag)	MOS (kms ⁻¹)	K97 (kms ⁻¹)	K00 (kms ⁻¹)	M90 (kms ⁻¹)
5066	443.2	404.1	12 30 50.9	12 23 48	21	20	1478
5067	434.4	400.1	12 30 51.2	12 23 40	26	12	1173
5071	368.1	428.9	12 30 49.3	12 22 32	-2	-56	1767
6003	-3.6	132.6	12 31 10.1	12 16 28	304	-420	20.62	1.19	1741	...
6004	-30.9	131.8	12 31 10.2	12 16 01	305	-447	20.92	1.10	1741	...
7001	722.2	912.6	12 30 15.7	12 28 15	-494	287	18.66	0.68	52 ± 111
7002	109.6	906.8	12 30 17.1	12 18 02	-474	-326	19.67	0.54	-329 ± 111
7003	368.9	895.7	12 30 17.4	12 22 22	-469	-66	18.50	1.64	-310 ± 181
7004	458.2	893.2	12 30 17.4	12 23 51	-468	23	21.52	1.05	1786 ± 174
7005	1.5	880.0	12 30 19.1	12 16 14	-444	-434	20.90	0.55	-16 ± 105
7006	530.3	865.8	12 30 19.2	12 25 04	-442	96	20.87	1.13	104 ± 58
7007	715.4	859.4	12 30 19.3	12 28 09	-440	281	21.16	1.18	138 ± 94
7008	232.9	867.2	12 30 19.6	12 20 06	-437	-202	21.67	2.33	2227 ± 142
7009	719.0	850.6	12 30 19.9	12 28 13	-432	285	19.84	1.93	1492 ± 78
7010	481.2	841.5	12 30 20.9	12 24 15	-417	47	17.32	3.14	133 ± 71
7011	874.1	829.4	12 30 21.1	12 30 49	-414	441	20.65	1.27	964 ± 179
7012	412.0	839.9	12 30 21.2	12 23 06	-414	-22	21.89	0.92	1205 ± 141
7013	852.5	810.9	12 30 22.4	12 30 28	-395	420	20.77	1.36	1004 ± 101
7014	907.1	781.4	12 30 24.3	12 31 23	-367	475	19.47	2.44	160 ± 90
7015	884.9	771.4	12 30 25.1	12 31 01	-356	453	19.78	1.14	-240 ± 108
7016	-25.3	719.4	12 30 30.1	12 15 52	-283	-456	20.99	1.21	1902 ± 100
7017	798.8	644.2	12 30 33.9	12 29 38	-227	370	20.06	2.17	94 ± 101
7018	-7.1	621.7	12 30 36.7	12 16 12	-186	-436	18.91	1.69	-8 ± 43
7019	492.9	488.4	12 30 45.0	12 24 36	-64	68	20.30	2.03	1589 ± 153
7020	412.9	480.4	12 30 45.7	12 23 16	-54	-12	19.54	1.80	1231 ± 89
7021	-52.5	475.2	12 30 46.8	12 15 30	-38	-478	19.63	1.41	1225 ± 88
7022	-1.4	463.8	12 30 47.5	12 16 22	-28	-426	21.41	1.09	-373 ± 184
7023	-51.1	458.7	12 30 47.9	12 15 32	-21	-476	21.04	1.70	415 ± 134
7024	475.6	427.0	12 30 49.2	12 24 20	-2	52	19.94	1.17	1632
7025	-39.3	-2.8	12 31 19.4	12 15 56	440	-452	19.94	1.69	1463 ± 69
7026	391.0	-16.2	12 31 19.6	12 23 06	443	-22	20.22	0.84	2 ± 110
7027	179.1	-26.0	12 31 20.7	12 19 35	458	-233	19.70	1.42	72 ± 61
7028	180.0	-48.5	12 31 22.2	12 19 36	481	-232	20.91	1.21	1345 ± 91
8001	87.4	224.8	12 31 03.7	12 17 57	209	-331	18.70	2.93	159 ± 127	not given
8002	203.2	452.9	12 30 47.9	12 19 47	-22	-221	20.52	1.39	1565 ± 144	not given
8003	216.4	248.1	12 31 01.9	12 20 05	183	-203	20.87	1.24	1355 ± 122
8004	475.6	480.5	12 30 45.6	12 24 19	-56	51	20.10	1.51	1658 ± 139
8005	478.4	471.6	12 30 46.2	12 24 22	-47	54	19.80	1.34	...	1934
8006	478.4	464.7	12 30 46.7	12 24 22	-40	54	19.80	1.35	1032 ± 107	1109
8007	772.6	531.3	12 30 41.6	12 29 15	-114	347	19.46	1.58	1183 ± 32	1106
8008	794.8	592.8	12 30 37.4	12 29 35	-176	367	20.36	1.37	...	1296
8051	439.6	622.6	12 30 36.0	12 23 39	-197	11	20.76	1.35	...	915
8052	489.8	407.4	12 30 50.6	12 24 35	17	67	1477
8053	646.7	251.3	12 31 01.0	12 27 16	169	228	15
8054	478.8	300.2	12 30 57.9	12 24 26	125	58	19.95	1.73	...	1169
8055	255.5	363.8	12 30 53.9	12 20 41	66	-167	20.59	1.58	...	467
8056	425.9	495.3	12 30 44.7	12 23 29	-69	1	20.04	1.78	...	1368
9001	480.5	636.7	12 30 34.9	12 24 20	-212	52	1338
9002	545.7	495.1	12 30 44.5	12 25 29	-72	121	1100
9051	363.7	437.2	12 30 48.7	12 22 28	-10	-60	1879
9052	320.5	427.7	12 30 49.5	12 21 45	1	-103	1763 ± 127	1480
9053	796.0	433.1	12 30 48.3	12 29 41	-16	373	796

TABLE 2
REVISED IDENTIFICATION NUMBERS.

Old ID	New ID	Comments
354	8001	Double, unresolved in S81; unique MOS target identified
408	8003	Double, unresolved in S81; unique MOS target identified
410	8053	Double, unresolved in S81; Keck target; both components blue
526	8054	Double, unresolved in S81; Keck target; both components red
715	8055	Very close double, unresolved in S81; Keck target; both components red
827	8052	Double, unresolved in S81; Keck target; both components red
868	9052	No reliable photometry; cosmic ray in photometric database?
881	9053	No reliable photometry
892	9051	No entry in photometry database; clearly seen in M87 direct frames
944	8002	Double, unresolved in S81; unique MOS target identified
978	8006	Multiple, unresolved in S81; reported twice in K97; unique MOS target identified
1013	8004	Double, unresolved in S81; unique MOS target identified
1065	9002	Double, unresolved in S81; Keck target; one component blue, one red
1067	8056	Very close double, unresolved in S81; Keck target; both components red
1180	8007	Double, unresolved in S81; unique MOS target identified
1340	8008	Double, unresolved in S81; unique MOS target identified
1400	8051	Very close double, unresolved in S81; Keck target; both components blue
1425	9001	Double, unresolved in S81; Keck target; one component blue, one red
5003	5053	No photometry
5005	5055	No photometry
5008	5058	No photometry
5014	5064	No photometry
5015	5065	No photometry
5016	5066	No photometry
5017	5067	No photometry
5021	5071	No photometry
5024	8006	Recognized as redundant listing of 978 in K97; see entry above
5026	8005	Multiple, part of unresolved target 978 in S81; given twice in K97; merged

TABLE 3
PROPERTIES OF THE MOS DETECTOR AND GRISM.

Item	Attribute
Detector	2048x2048 STIS2 CCD
Image Scale	0".44 per 21μ pixel
QE	0.85 at 5200\AA
Read Noise	~ 9 electrons
Field of View	~ 9.5 arcmin
Grism	B400
Zero Deviation	5186\AA
Dispersion	3.59\AA per pixel
Filter central wavelength	5100\AA
Filter bandwidth	1200\AA

TABLE 4
GALACTIC GLOBULAR CLUSTERS USED AS TEMPLATES.

Cluster	[Fe/H] ^a (dex)	Heliocentric velocity ^a (km/s)
NGC6171	-1.04	-33.6
NGC6205	-1.54	-246.6
NGC6356	-0.50	27.0
NGC6402	-1.39	-66.1
NGC6528	-0.17	184.9
NGC6624	-0.42	53.9

^a Harris (1996).

TABLE 5
SPECTROSCOPIC FRAMES OF THE M87 GCS.

Field	Exposure time	Airmass	Comments
Central 1	2 x 3600s (Night 2)	1.03 – 1.12	Scattered light; some cloud.
Central 2	2 x 3600s (Night 2)	1.13 – 1.88	Scattered light; some cloud.
Central 2	1 x 3600s (Night 3)	1.03 – 1.02	Scattered light.
Southeast	2 x 3600s (Night 3)	1.02 – 1.25	Scattered light, humid, poor seeing.
Southeast	2 x 3600s (Night 4)	1.14 – 1.85	Scattered light eliminated
Northwest	2 x 3600s (Night 4)	1.01 – 1.10	Mask slightly rotated; about 50% of targets on slitlets.
Northwest	2 x 3600s (Night 5)	1.01 – 1.15	New NW mask cut and mounted; no problems.
Southwest	2 x 3600s (Night 5)	1.21 – 2.10	No problems.

This figure "m87paper1-fig07.jpg" is available in "jpg" format from:

<http://arxiv.org/ps/astro-ph/0106004v1>